



OPEN **Spatial and temporal patterns of precipitation concentration and their associated risks**

Xinhao Suo¹, Yongye Jiang¹, Guolong Chen¹, Jingyi Li¹, Yuqin Lai¹, Longsheng Li¹, Mengmeng Lu¹, Xinyi Wang¹, Bo Fu²✉ & Bengang Li¹✉

Global climate change has profoundly altered precipitation distribution patterns, with the “Wet getting Wetter, Dry getting Drier” (WWDD) pattern widely recognized. However, most previous studies have addressed either the temporal or spatial dimensions of precipitation concentration in isolation, leaving a critical gap in understanding their finer-scale changes and their combined effects and interactive risks. Here, we use the Gini coefficient and ERA5-Land daily data (1951–2020) to assess global precipitation concentration in both time and space. Based on long-term trends, we classify regions into WWDD or WDDW patterns. Our results reveal that 46.4% of global land area shows increasing spatial concentration (WWDD), while 67.4% shows increasing temporal concentration (WWDD). Notably, 33.6% of the global land area exhibits a WWDD pattern in both spatial and temporal dimensions. These jointly concentrated regions are especially vulnerable, as precipitation is becoming more uneven in both time and space, increasing the risk of floods, droughts, and other extreme hydrometeorological events. In contrast, regions with increasing concentration in only one dimension may face more specific hazards—such as short-duration intense precipitation or localized runoff surges. These findings have important implications for assessing global precipitation concentration and informing hydrological disaster management strategies.

Global climate change has significantly altered the distribution of precipitation worldwide, posing serious challenges to socioeconomic development and ecosystem stability^{1,2}. Greater precipitation concentration increases the likelihood of extreme events, including droughts, floods, and other climate-related disasters^{3–5}. Therefore, a deeper understanding of precipitation distribution patterns is crucial for developing timely and effective adaptation strategies to reduce the negative impacts on both human societies and ecosystems^{6–9}.

Numerous studies have explored the “wet becoming wetter and dry becoming drier” (WWDD) phenomenon from a temporal perspective, revealing that many regions experience “wet seasons becoming wetter and dry seasons becoming drier”¹⁰. For instance, Zhou et al. found that global warming intensifies the seasonality of the hydrological cycle, with wet seasons becoming wetter and dry seasons drier, as evidenced by their analysis of surface water availability¹¹. Similarly, Chou et al. observed a “wet-get-wetter” pattern in humid regions, while arid areas exhibited a “dry-get-drier” trend during their respective dry seasons¹². Other studies have also highlighted an intensification of precipitation during wet seasons compared to dry seasons^{13,14}. However, most of these investigations have concentrated on seasonal scales, leaving daily-scale precipitation changes largely underexplored. This gap implies that short-duration, intense precipitation events remain insufficiently understood. Precipitation concentration at the daily scale implies more abrupt and short-duration changes, which may lead to disasters such as flash floods or intense short-term precipitation. Such events are harder to predict and pose heightened risks to public safety and infrastructure.

In addition, many studies have assessed the WWDD phenomenon from a spatial perspective, focusing on contrasts between wet and dry regions. For instance, Greve et al. estimated that only 10.8% of the global land area exhibits the WWDD pattern, whereas Yang et al. found this pattern in more than 20% of land areas^{15,16}. Trancoso et al. employed ensembles of Global Climate Model (GCM) to identify robust signals of both drying and wetting trends and to quantify population exposure under various emission scenarios¹⁷. Although these spatial patterns have been well documented at regional scales, changes in precipitation distribution within regions remain insufficiently explored. This fine-scale hydrological shift could lead to localized flooding events, presenting significant challenges for regional water management.

¹Institute of Carbon Neutrality, Sino-French Institute for Earth System Science, College of Urban and Environmental Sciences, Peking University, Beijing 100871, China. ²Institute of Reproductive and Child Health, School of Public Health, Peking University, Beijing 100191, China. ✉email: pkufubo@pku.edu.cn; libengang@pku.edu.cn

The WWDD phenomenon in space or time is often discussed separately. Benjamin et al. comprehensively reviewed the applicability and limitations of the temporal or spatial WWDD pattern in different frameworks, scales, and contexts¹⁸. Although the progress in research on both scales has been thoroughly analyzed, few studies have investigated the combined results of these two scales. Whether in the temporal or spatial dimension, WWDD indicates that certain areas or periods are at risk of drought or extreme precipitation. Notably, the combination of these WWDD phenomena amplifies the effects of uneven precipitation distribution, significantly increasing the likelihood of extreme droughts or floods.

To address existing research gaps, this study aims to identify the current spatial and temporal patterns of precipitation concentration across different regions, and to trace their historical trends from 1951 to 2020 using the Gini coefficient. This enables us to differentiate between the dominant “Wet getting Wetter, Dry getting Drier” (WWDD) pattern and the contrasting “Wet getting Drier, Dry getting Wetter” (WDDW) pattern. By combining temporal and spatial dimensions, this approach offers a more comprehensive understanding of evolving hydroclimatic extremes. This spatiotemporal coupling framework not only refines the analytical framework for assessing precipitation concentration, but also highlights regions experiencing simultaneous intensification in both temporal and spatial dimensions. These regions are particularly vulnerable to compound hydrological extremes, such as the flash floods and prolonged droughts. By identifying regions with dual concentration trends, our findings offer concrete guidance for regional decision-makers to implement adaptive strategies, including early-warning systems, infrastructure planning, and water resource management. This marks a shift from broad global assessments toward more targeted, actionable insights for enhancing climate resilience.

Materials and methods

Temporal coefficients

Reanalysis data is characterized by its broad spatial coverage and high temporal resolution. In this study, we used daily ERA5-Land dataset (1951–2020)¹⁹ which provides a consistent description of the evolution of water and energy cycles over land, making it an essential resource for analyzing trends and anomalies^{20,21}. In this study, the selected variable is total precipitation, with the daily precipitation at 00:00 representing the accumulated precipitation for the entire day. According to the ETCCDI definition, days with less than 1 mm/day of precipitation were classified as non-rainy, allowing us to distinguish between rainy and non-rainy days (<https://etccdi.pacificclimate.org/>). The ERA5-Land dataset spans from 1950 to the present, effectively addressing the challenge of providing consistent global precipitation simulations on a worldwide scale²¹. Recent studies have shown that ERA5-Land outperforms other reanalysis datasets or its predecessor ERA5 in terms of performance at the global level, offering higher spatial and temporal resolution^{19,22,23}. However, it should be noted that this study focuses on global-scale analysis, if the objective were to analyze only a specific region, more regionally datasets might provide greater accuracy^{24–26}.

The Gini coefficient, originally developed to measure income inequality, has been effectively adapted to reflect the distribution of precipitation concentration. Drawing inspiration from its application in economic studies, we used the Gini coefficient to evaluate precipitation concentration, focusing on its distribution among. However, the traditional calculation of the annual Gini coefficient can be heavily influenced by the number of non-rainy days, which tend to skew the measure towards greater inequality when they constitute a large proportion of the days. This occurs because a high number of zero precipitation days makes the Lorenz curve veer toward the bottom-left corner of the equality line, indicating that most precipitation falls on relatively few rainy days (Supplementary Figure S1). Given this bias, our assessment specifically utilized the Gini coefficient for rainy days only (Eq. 1)²⁷.

Drought will have adverse effects on agricultural production, vegetation growth, and human society²⁸. Suraj D. Polade et al. identified the key role of dry days in altering regional climate and precipitation regimes, showing that in much of the subtropics, changes in the number of dry days dominate annual variations in precipitation and contribute significantly to interannual precipitation variability²⁹. However, since the precipitation on dry days is zero, with only the number of dry days having significance but not their magnitude, the Gini coefficient cannot be used to reflect the annual concentration of dry days. Therefore, we use the ratio of non-rainy days to total days to represent the importance of dry days (Eq. 2). A high ratio signifies fewer rainy days, suggesting that precipitation is concentrated within those days. Conversely, a lower ratio indicates a more even distribution of precipitation throughout the year (Supplementary Figure S1).

To provide a comprehensive measure of annual precipitation concentration, we combined both indicators, which range from 0 to 1, by averaging them (Eq. 3). This method acknowledges the influence of both the volume of rain on rainy days and the frequency of those days, offering a more nuanced insight into yearly precipitation patterns. Where x_i is the amount of precipitation on the i day, and n_{rainy} is the number of total precipitation days.

$$rainyday_coefficient = \frac{1}{n_{rainy}} \cdot \frac{\sum_{i=1}^{n_{rainy}} (2i - n_{rainy} - 1) \cdot x_i}{\sum_{i=1}^{n_{rainy}} x_i} \quad (1)$$

$$nonrainyday_coefficient = n_{nonrainy}/(n_{nonrainy} + n_{rainy}) \quad (2)$$

$$Temporal_coefficient = \frac{rainyday_coefficient + nonrainyday_coefficient}{2} \quad (3)$$

Based on the regional divisions from the IPCC Sixth Assessment Report (AR6), we classified the world into 44 regions³⁰ (Table 1). For each region, we first calculated the rainy day and non-rainy day coefficients at the grid level, then averaged these coefficients over the region to obtain the regional mean values. The average of these two coefficients was then used to calculate the regional annual temporal coefficient.

No.	Region names	Abbreviation	No.	Region names	Abbreviation
1	Greenland/Iceland	GIC	23	Central-Africa	CAF
2	N.W.North-America	NWN	24	N.Eastern-Africa	NEAF
3	N.E.North-America	NEN	25	S.Eastern-Africa	SEAF
4	W.North-America	WNA	26	W.Southern-Africa	WSAF
5	C.North-America	CNA	27	E.Southern-Africa	ESAF
6	E.North-America	ENA	28	Madagascar	MDG
7	N.Central-America	NCA	29	Russian-Arctic	RAR
8	S.Central-America	SCA	30	W.Siberia	WSB
9	Caribbean	CAR	31	E.Siberia	ESB
10	N.W.South-America	NWS	32	Russian-Far-East	RFE
11	N.South-America	NSA	33	W.C.Asia	WCA
12	N.E.South-America	NES	34	E.C.Asia	ECA
13	South-American-Monsoon	SAM	35	Tibetan-Plateau	TIB
14	S.W.South-America	SWS	36	E.Asia	EAS
15	S.E.South-America	SES	37	Arabian-Peninsula	ARP
16	S.South-America	SSA	38	S.Asia	SAS
17	N.Europe	NEU	39	S.E.Asia	SEA
18	West&Central-Europe	WCE	40	N.Australia	NAU
19	E.Europe	EEU	41	C.Australia	CAU
20	Mediterranean	MED	42	E.Australia	EAU
21	Sahara	SAH	43	S.Australia	SAU
22	Western-Africa	WAF	44	New-Zealand	NZ

Table 1. Names and abbreviations of the 44 land regions.

A value closer to 1 indicates that precipitation is concentrated on a few days within the year, while a value closer to 0 suggests a more even distribution of precipitation throughout the year (Supplementary Figure S2). A positive trend indicates that precipitation is becoming more concentrated, reflecting the phenomenon of “wet days getting wetter and dry days getting drier,” while a negative trend suggests a shift toward more evenly distributed precipitation, reflecting the phenomenon of “wet days becoming drier and dry days becoming wetter” (Supplementary Figure S2). It is important to note that the WWDD phenomenon refers to relative changes.

Spatial coefficients

For the spatial Gini coefficient of each region, we first calculated the annual precipitation for each grid using ERA5, which allowed us to derive the cumulative distribution of precipitation across the region’s grids. Based on this distribution, we computed the annual regional Gini coefficient (Eq. 4). A higher Gini coefficient indicates that precipitation is more concentrated in a few grids, while a value closer to 0 suggests a more uniform distribution of precipitation. A positive trend indicates that precipitation is becoming increasingly concentrated, reflecting the phenomenon of “wet areas getting wetter and dry areas getting drier.” Conversely, a negative trend suggests that precipitation is becoming more evenly distributed, i.e., “wet areas becoming drier and dry areas becoming wetter”. Where X_j is the amount of precipitation on the j grid, and n_{grids} is the number of grids in the region.

$$\text{Spatial coefficient} = \frac{1}{n_{\text{grids}}} \cdot \frac{\sum_{j=1}^{n_{\text{grids}}} (2j - n_{\text{grids}} - 1) \cdot X_j}{\sum_{j=1}^{n_{\text{grids}}} X_j} \quad (4)$$

Trend analysis

This study focuses on assessing changes in precipitation concentration (Gini coefficient), specifically identifying “Wet getting Wetter, Dry getting Drier” (WWDD) patterns. Accordingly, Ordinary Least Squares (OLS) linear regression was selected as the primary analytical method. While it may underestimate nonlinear trends in regions with high variability—such as monsoon-influenced areas—its results are intuitive and facilitate cross-regional comparisons due to the standardized units. Nonetheless, future research could incorporate more sophisticated approaches, such as piecewise regression or machine learning techniques (e.g., Random Forest), to better capture complex or nonlinear trend patterns. For trend analysis, both temporal and spatial scales are based on the annual Gini coefficients of precipitation concentration. Specifically, a linear model is established between the Gini coefficient y at each spatial grid point (or time series) and the time variable t :

$$y = \alpha + \beta t + \epsilon \quad (5)$$

where α is the intercept, β is the slope (representing the rate of change), and ϵ is the residual term. The sign and magnitude of the slope β indicate the direction and strength of the trend (e.g., if $\beta > 0$, the Gini coefficient

increases over time). In this study, the significant confidence levels of time-related linear trends are estimated using 95%, 99%, and 99.9% Student's t-test confidence level.

Results

Spatial patterns and trends in precipitation concentration

Between 2001 and 2020, the precipitation patterns in the SAH, ARP, ECA, and CAU regions exhibited high spatial concentration, as indicated by exceptionally high Gini coefficient values of 0.99, 0.99, 0.85, and 0.82, respectively (Fig. 1a; Table 1). These values suggest that precipitation was highly unevenly distributed in these regions, with a significant fraction of the total precipitation concentrated at a small number of locations³¹. This pattern may be attributed to regional climatological factors, such as monsoon systems or complex interactions between local topography and atmospheric circulation^{32–34}. In contrast, the ENA region showed a much more uniform precipitation distribution, as reflected by its notably lower Gini coefficient of 0.10 (Fig. 1a). This lower value indicates a more even spread of precipitation across the region, potentially reflecting more stable and evenly distributed weather systems.

The trend in the Gini coefficient also has critical implications for understanding regional precipitation patterns, particularly in relation to the WWDD and WDDW phenomena. Our results show that in half of the 44 regions studied (accounting for 46.4% of the global land area), the Gini coefficient increased, indicating a shift towards a more uneven precipitation distribution and suggesting a WWDD pattern. The NEAF region exhibited

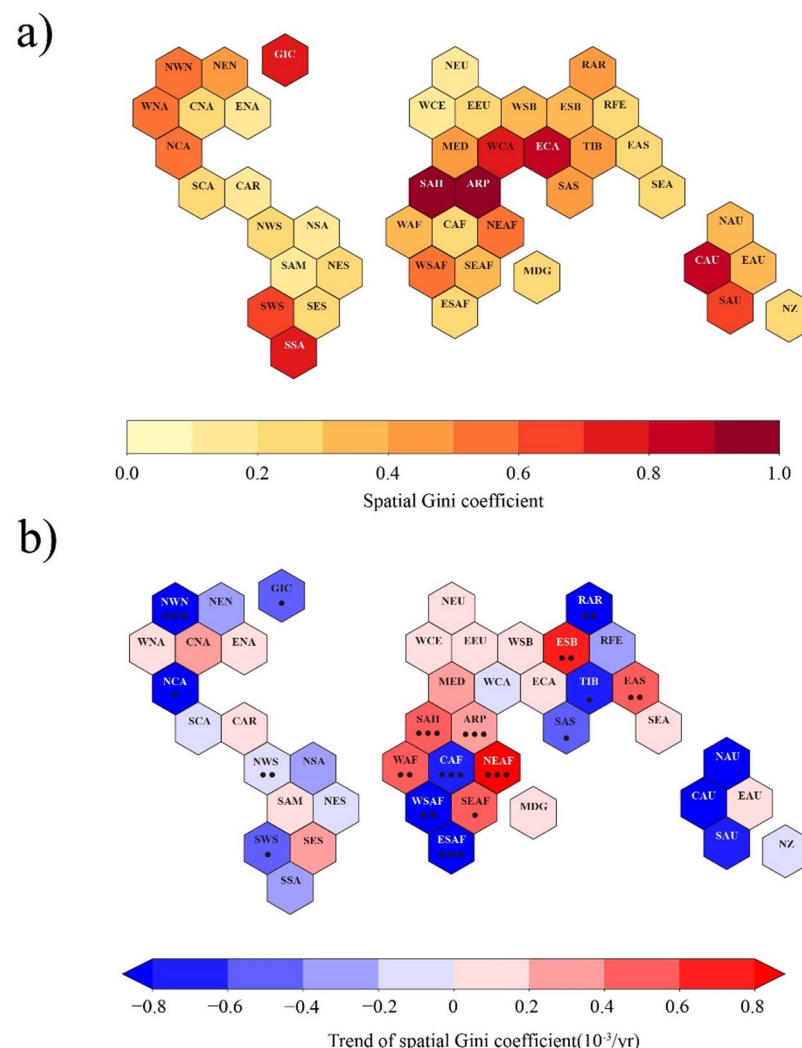


Fig. 1. Current spatial Gini coefficient and its trend (1951–2020) across the different regions. (a) Current spatial Gini coefficient. The values represent the mean spatial Gini coefficient for 2001–2020. Darker colors indicate more concentrated precipitation distribution within a region, whereas lighter colors represent a more uniform distribution of precipitation. (b) Trend of spatial Gini coefficient. The results show the historical trend from 1951 to 2020. Red indicates a positive trend, meaning “wet areas get wetter and dry areas get drier” while blue indicates a negative trend, meaning “wet areas become drier and dry areas get wetter”. (Symbols indicate statistical significance: · for $p < 0.05$, .. for $p < 0.01$, and ... for $p < 0.001$).

the most notable WWDD pattern ($p < 0.001$), characterized by a significant upward trend in the spatial Gini coefficient $1.4 \times 10^{-3} \text{ yr}^{-1}$ (Fig. 1b). In NEAF, wetter areas received more precipitation over time, while drier areas became even drier. This divergence amplified disparities, resulting in an increasingly uneven precipitation distribution within the region (Supplementary Figure S3). And the precipitation trends at grid scale in other regions are shown in Supplementary Figures S4 and S5.

Conversely, the other 22 regions exhibited a decreasing Gini coefficient trend, indicating the emergence of the WDDW pattern, in which the precipitation distribution becomes more even over time. Among them, 11 regions showed statistically significant declines, with WSAF experiencing the largest decrease in Gini coefficient ($-1.7 \times 10^{-3} \text{ yr}^{-1}$) (Fig. 1b). Similar to NEAF, this region encompasses both tropical desert and tropical savanna climates³⁵. However, the WSAF experienced increased precipitation in drier areas and decreased precipitation in wetter areas (Supplementary Figure S3). These changes may be attributed to alterations in atmospheric circulation patterns and regional climate dynamics driven by global climate change^{31,36}. Overall, although African regions share a mix of high- and low-precipitation climate types, they clearly exhibit starkly contrasting trends in wetness and dryness. WAF, NEAF, and SEAF all fall within the tropical monsoon climate zone, where seasonal shifts in monsoon winds are the main driver of precipitation patterns³⁷. However, with climate change, a weakening of the monsoon system has been observed in these regions, leading to a reduction in precipitation. In contrast, CAF, which is partially situated in the tropical monsoon zone, exhibited a different trend. In the CAF region, a general decrease in precipitation has been observed³⁷ but precipitation is distributed more evenly across the region, resulting in the WDDW pattern. The WSAF and ESAF regions, which occur outside the tropical monsoon zone, exhibited an increasing precipitation trend, with more evenly distributed precipitation across the region. Unlike regions dependent on monsoon systems, WSAF and ESAF benefit from more stable and consistent precipitation regimes, which may help reduce the risk of extreme dry periods. In Asia, particular attention is warranted for the EAS and ESB regions, where wet areas are becoming wetter while dry areas are becoming drier. These densely populated regions face heightened exposure to hydrometeorological disasters due to increasing precipitation concentration³³. As such, greater attention should be paid to flood events caused by runoff convergence resulting from spatially concentrated precipitation.

Temporal patterns and trends in precipitation concentration

The temporal Gini coefficient reflects the degree to which precipitation is concentrated throughout the year. We found relatively small regional differences in the temporal Gini coefficient. Among these regions, CAU and ECA showed the highest temporal Gini coefficients (0.69 and 0.64, respectively), reflecting more uneven precipitation distributions (Figs. 2a and 3a). Specifically, CAU and ECA exhibited notably high rainy-day coefficient values of 0.46 and 0.40, respectively, indicating that not only is precipitation concentrated throughout the year, but it is also clustered within a limited number of rainy days (Fig. 3c). This is further exacerbated by high non-rainy-day coefficients (0.91 and 0.87), suggesting long dry spells throughout the year, increasing vulnerability to water scarcity and droughts (Fig. 3c). In contrast, SEA had a much lower temporal Gini coefficient (0.17), indicating a markedly more uniform precipitation pattern (Figs. 2a and 3c). This low value suggests a more evenly distributed precipitation pattern, with precipitation spread evenly across the year. SEA also had the lowest non-rainy-day coefficient (0.21), indicating infrequent and short dry periods (Fig. 3c). The value of the rainy-day coefficient in SEA was also exceptionally low (0.13), suggesting that precipitation events are generally spread and less concentrated on any given day (Fig. 3c). This uniformity in precipitation supports stable water availability, with important ecological and agricultural benefits. This consistency in precipitation is beneficial for agricultural planning and water resource management, as it reduces the likelihood of severe drought events.

The temporal Gini coefficient trends revealed a notable pattern across many regions where the WWDD phenomenon occurs. This phenomenon is indicative of more extreme precipitation events, which are becoming increasingly concentrated on fewer, wetter days. Among the 44 regions, 33 exhibited an increasing temporal Gini coefficient value, accounting for 67.4% of the total land surface, indicating a growing imbalance in the temporal distribution of precipitation. Among these regions, 14 showed statistically significant changes ($p < 0.05$), highlighting the robustness of this trend in most of the regions examined (Figs. 2b and 3b).

Regions such as SEAF and NEAF exhibited the most pronounced WWDD trends, with temporal Gini coefficient rates of $0.8 \times 10^{-3} \text{ yr}^{-1}$ and $0.9 \times 10^{-3} \text{ yr}^{-1}$, respectively (Figs. 2b and 3b). In these regions, both the rainy-day coefficient and the number of non-rainy days are increasing, suggesting that precipitation is becoming more concentrated throughout the year (Fig. 3c). The rising number of non-rainy days points to increased drought frequency, while the elevated rainy-day coefficient reflects a growing tendency for extreme rainfall to be confined to fewer days. This combination reflects a growing vulnerability to both droughts and sudden, heavy precipitation events. The observed WWDD trend in SEAF and NEAF also suggests a shift towards a more extreme climate in these regions, with the potential for the occurrence of higher-intensity floods or drought events. Agriculture in these regions may face increasing challenges and require more adaptive irrigation systems and improved flood control mechanisms to mitigate the risks associated with these shifts^{32,34,38}. Urban regions in these areas may also need upgraded drainage infrastructure to accommodate more frequent and intense rainfall events³⁹⁻⁴¹. In contrast, regions such as NSA and WSAF also exhibited a general WWDD pattern, but the underlying drivers of this trend are different (Figs. 2b and 3c). In these regions, the WWDD pattern is driven primarily by more concentrated precipitation on rainy days, while the non-rainy-day coefficient value decreases. This suggests that precipitation is redistributed across more days and that fewer non-rainy days occur.

Interestingly, 11 regions exhibited the opposite pattern, namely, identified as the WDDW pattern, with statistically significant changes observed in four of these regions (Figs. 2b and 3c). This reversal of the WWDD pattern was primarily driven by a significant reduction in the number of non-rainy days, indicating a more even temporal distribution of precipitation throughout the year. In these regions, while precipitation on individual rainy days is becoming more concentrated, the overall temporal Gini coefficient value decreases (Fig. 3c). This

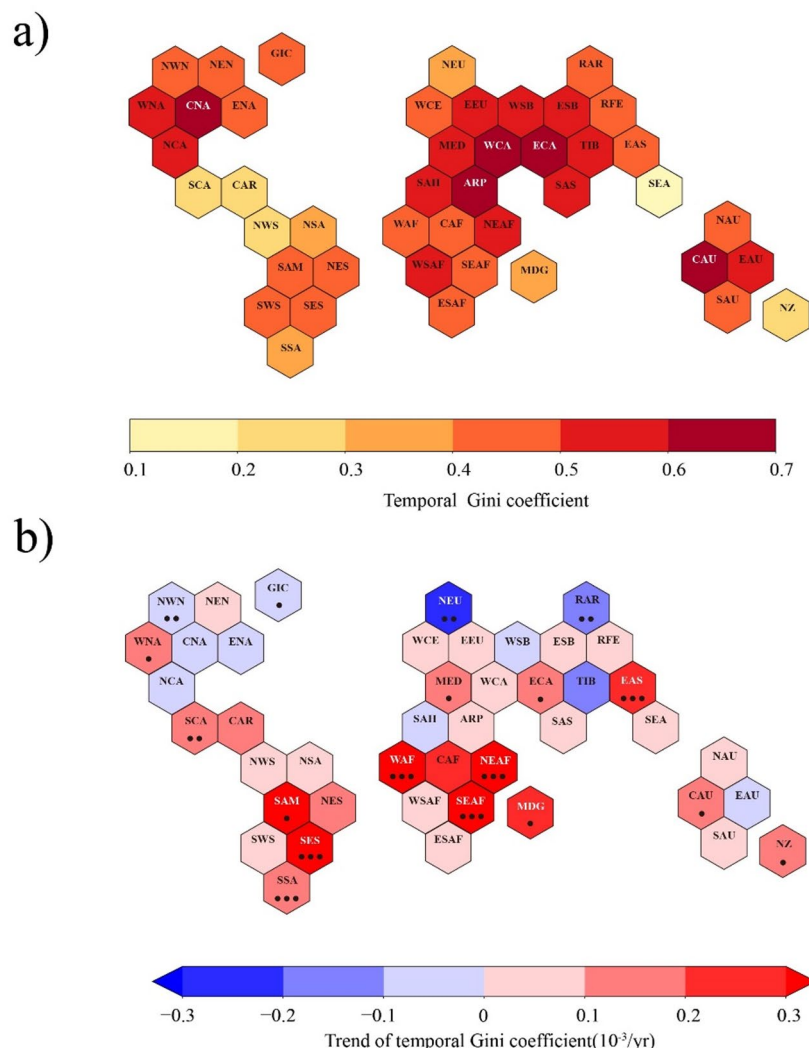


Fig. 2. Current temporal Gini coefficient and its trend (1951–2020) across the different regions. (a) Current temporal Gini coefficient. The values represent the mean temporal Gini coefficient for 2001–2020. It is the average of the coefficient on rainy days and the coefficient on non-rainy days. Darker colors indicate more concentrated precipitation distribution within a region, whereas lighter colors represent a more uniform distribution of precipitation. (b) Trend of spatial Gini coefficient. The results show the historical trend from 1951 to 2020. Red indicates a positive trend, meaning “wet areas get wetter and dry areas get drier” while blue indicates a negative trend, meaning “wet areas become drier and dry areas get wetter”. (Symbols indicate statistical significance: • for $p < 0.05$, .. for $p < 0.01$, and ... for $p < 0.001$).

suggests that while these regions still experience extreme precipitation events on certain days, the reduction in dry periods reduces the occurrence of prolonged droughts.

In summary, the temporal Gini coefficient trends reveal pronounced regional disparities in precipitation patterns, which are critical for understanding future climate change across different regions. The WWDD and WDDW patterns represent two major patterns of precipitation concentration. Beyond assessing the overall trends, it is essential to jointly consider the concentration of precipitation on rainy days and the frequency of non-rainy days to comprehensively evaluate the precipitation distribution risks faced by each region. These insights are vital for formulating region-specific climate adaptation strategies.

Coupling of the spatial–temporal variation trends in precipitation

Assessing the WWDD phenomenon solely from either a spatial or temporal perspective limits the ability to comprehensively evaluate the disaster risks associated with precipitation concentration across different regions. To address this limitation, we integrated changes in the precipitation distribution across both spatial and temporal scales, thereby categorizing the global distribution into four types: WWDD_{Spatial-Temporal} (precipitation is concentrated at both the spatial and temporal scales), WWDD_{Temporal} (precipitation is concentrated at the temporal scale), WWDD_{Spatial} (precipitation is concentrated at the spatial scale), and WDDW_{Spatial-Temporal} (precipitation exhibits evenness at both the spatial and temporal scales).

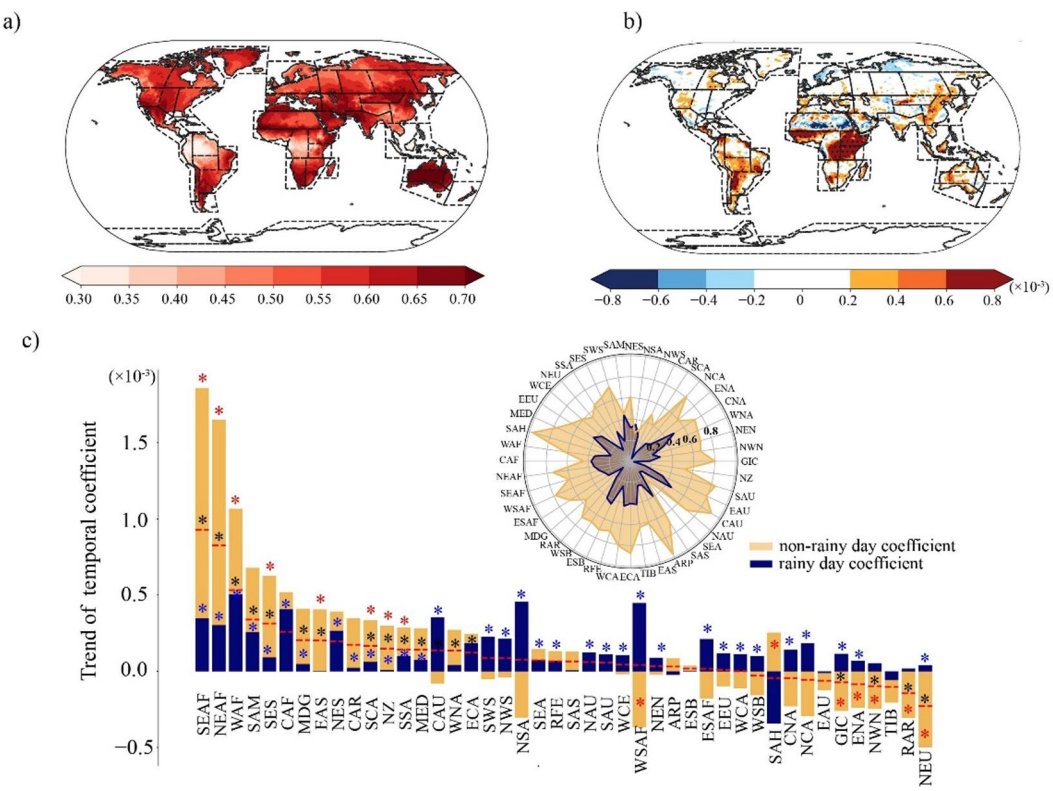


Fig. 3. Spatial pattern and trends of temporal coefficient. (a) The mean value of temporal coefficient (2001–2020). Darker colors indicate higher precipitation concentration, signifying more uneven distribution of annual precipitation within grids. (b) The Trend of temporal coefficient (1951–2020). Red indicates a positive trend, meaning “wet days get wetter and dry days get drier” while blue indicates a negative trend, meaning “wet days get drier and dry days get wetter”. (c) Regional trends of temporal coefficient. Yellow bars represent the trend in the non-rainy days’ coefficient, blue bars represent the trend in the rainy days’ coefficient, and the red line indicates the trend of temporal coefficient. Regions are reordered based on the magnitude of the temporal coefficient trend, from largest to smallest. Statistically significant regions are marked with $^*(P < 0.05)$. The radar chart in (c) shows the regional average of the temporal coefficient from 2001 to 2020.

The results revealed that 16 regions demonstrated the WWDD phenomenon on both spatial and temporal scales (WWDD_{Spatial-Temporal}), including Asia (EAS, ESB, SEA, TIB, and ARP), North America (WNA and CAR), South America (SAM and SES), Europe (WCE, EEU, and MED), and Africa (WAF, EAF, NEAF, SEAF, and MDG), accounting for 33.6% of the global land area (Fig. 4a, c). The WWDD pattern clearly occurs worldwide, encompassing both developed and developing regions. These regions are confronting the dual challenge of more intense extreme precipitation, leading to flooding and infrastructure damage, and extended dry spells that exacerbate water scarcity. Conversely, five regions exhibited a WDDW pattern at both the spatial and temporal scales (WDDW_{Spatial-Temporal}). These regions are located primarily at middle and high latitudes in the Northern Hemisphere and include GIC, NWN, NCA, RAR, and TIB (Fig. 4a, c). The WDDW pattern in these regions could indicate a shift towards a more stable and predictable climate, which may have beneficial implications for agriculture and human habitation. Additionally, most regions in the Southern Hemisphere exhibited the phenomenon of “wet days becoming wetter but wet areas becoming drier” (WWDD_{Temporal}; Fig. 4a, c). The phenomenon of “wet days becoming drier but wet areas becoming wetter” primarily occurs in six regions near the Atlantic (WWDD_{Spatial}). These regions showed more evenly distributed precipitation throughout the year but an uneven distribution within each region (Fig. 4a, c). Spatially, the distribution of precipitation in these regions is becoming more uniform, and short-term extreme precipitation requires increased attention, especially in the NEU, ENA, EAU and other regions, which are economically developed and densely populated regions. Once extreme precipitation occurs in these regions, considerable economic losses can occur.

When we analysed the precipitation trend, we observed an issue of concern. In regard to the WWDD_{Spatial-Temporal} pattern, precipitation in nearly 70% of the regions is decreasing, whereas precipitation in the remaining regions is increasing, which demonstrates that although these regions are becoming wetter in terms of both the number of rainy days and wet areas, the risks are not consistent (Fig. 4b, c). Adopting NEAF and SEAF as examples, the total precipitation in these regions is decreasing, suggesting that, relative to that of wetter conditions, the risk of dry conditions becoming drier is greater (Fig. 4b, c). These regions will become less suitable for human habitation and agriculture. For example, as droughts increase, regions with this trend may experience reduced conditions for rainfed agriculture, and the availability of a reliable water

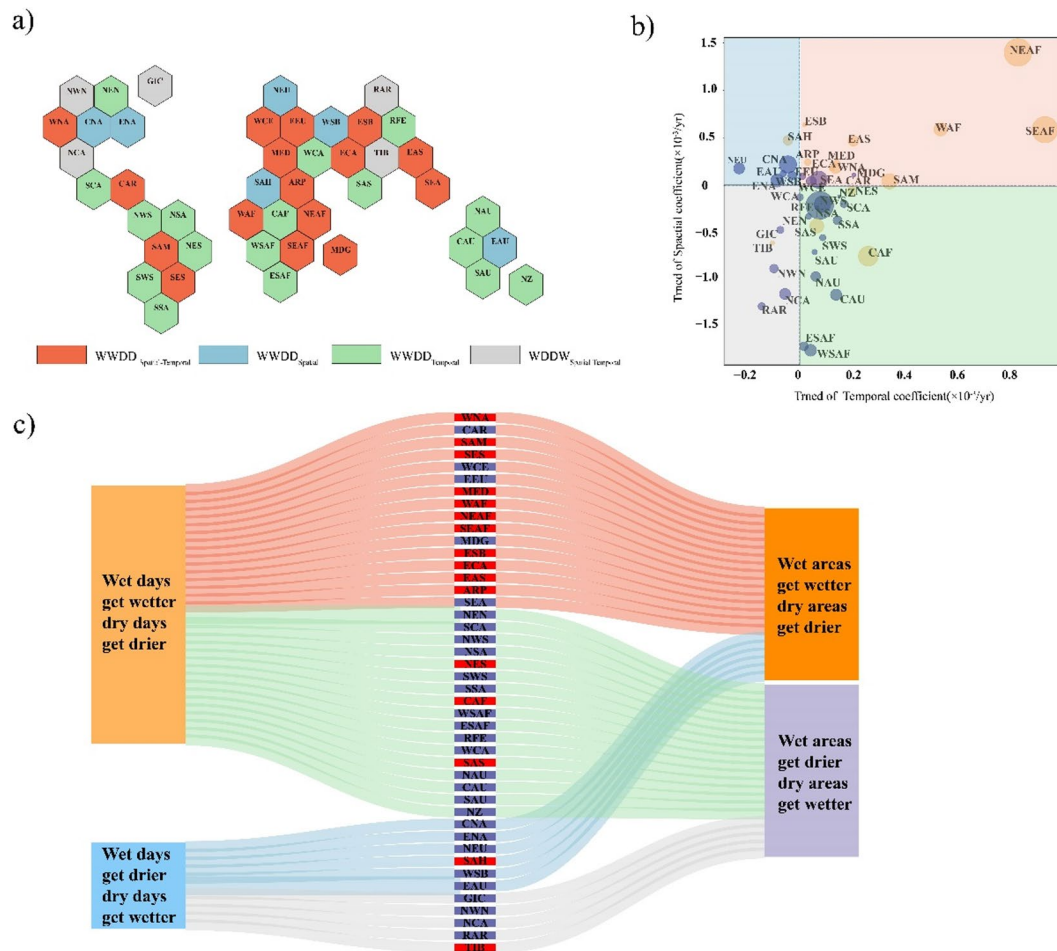


Fig. 4. Regional classification based on the spatiotemporal variation in the precipitation distribution. (a) Global risk partitioning. Regions are classified based on the occurrence of temporal and spatial WWDD patterns, included WWDD_{Spatial-Temporal} (red), WDDW_{Spatial-Temporal} (gray), WWDD_{Temporal} (green), and WDDW_{Spatial} (blue). (b) Global regional scatter plot. Regions in the first quadrant are classified as WWDD_{Spatial-Temporal} regions, those in the second quadrant as WWDD_{Spatial} regions, those in the third quadrant as WDDW_{Temporal} regions, and those in the fourth quadrant as WWDD_{Temporal} regions. The color of the scatter points indicates whether the precipitation trend is increasing (dark blue) or decreasing (yellow). The size of the scatter points represents the magnitude of absolute precipitation change, with larger diameters indicating greater absolute changes. (c) Sankey map of precipitation distribution change on temporal and spatial scales. The left side is the temporal scale, the right side is the spatial scale, and the middle is the name of the region. The color of the region indicates the change of precipitation, with blue indicating the increase of precipitation and red is decreasing.

supply for crop growth decreases, potentially rendering these regions even less attractive for agriculture and settlement^{34,38}. In contrast, SEA is experiencing an increase in the total precipitation. Thus, the risk of wetter conditions becoming wetter will increase, and more attention should be given to extreme precipitation and flood prevention in such regions (Fig. 4b, c). It is widely considered that with global warming, the overall amount of precipitation worldwide will increase¹. However, we generally observed the WWDD_{Spatial-Temporal} pattern in regions that do not conform to this phenomenon. Notably, decreasing precipitation more notably affects the occurrence of dry areas or days, possibly due to reduced water transport driven by subtropical anticyclones in the Northern Hemisphere and complex circulation patterns in the Southern Hemisphere⁴².

In terms of the WWDD_{Temporal} pattern, precipitation is increasing in most regions, accounting for 80% of the total land area, so more attention should be given to the occurrence of extreme precipitation events in urban or ecologically vulnerable areas (Fig. 4b, c). Other regions experienced a decrease in precipitation, such as CAF, SAS, and NES, indicating that light precipitation occurs less in these regions, which calls for greater attention to drought events throughout the year (Fig. 4b, c). In addition, in regard to the WWDD_{Spatial} pattern, precipitation in nearly all regions is increasing, which indicates that although the precipitation gap between wet and dry days has not decreased, wet areas are more susceptible to extreme precipitation (Fig. 4b, c). In these regions, it is essential to focus on flood events in areas with higher precipitation.

Discussion and conclusion

Accurately characterizing and predicting precipitation distributions has long posed a significant challenge in scientific research. Among existing challenges, the question of whether “wet regions are becoming wetter” or “all regions are becoming drier” has been widely debated¹⁸. This issue has significant implications for the management of extreme precipitation and the impacts of drought-related disasters^{43–45}.

Unlike previous studies that relied on precipitation amount or related variables, this study adopts the Gini coefficient to assess precipitation patterns. This enables a direct quantification of the degree of concentration. More importantly, our analysis captures changes in precipitation concentration within regions, providing more practical insights for local managers in disaster prevention and climate adaptation efforts. In this study, we employed the Gini coefficient of the regional precipitation to assess changes in intraregional precipitation patterns and analyse both temporal and spatial patterns (WWDD or WDDW) in different regions. Via this approach, we evaluated the degree of wet conditions becoming wetter across various grids and regions, thereby combining temporal- and spatial-scale analyses to examine the risks posed by changes in precipitation patterns in different regions. Our results, which are consistent with those of other studies, indicated that not all regions are exhibiting the “wet areas becoming wetter and dry areas becoming drier” phenomenon^{15,16}. Consistent with Greve, the WWDD phenomenon was observed in the ENA, EEU, SAM and other regions, whereas different results were observed in the NEAF, WAF and other regions¹⁵. Yang et al. reported consistent WWDD phenomena in the NEAF, ESB, SEA and other regions, whereas the opposite phenomenon was observed in the NWS and other regions¹⁶. The size of the WWDD region is smaller than the area determined in our study^{15,16}. Globally, half of the regions exhibited the WWDD pattern. In these regions, precipitation becomes more concentrated, leading to rapid runoff convergence and the occurrence of natural disasters such as floods^{44,45}. In contrast, regions characterized by the WDDW phenomenon exhibit more evenly distributed precipitation, rendering them increasingly suitable for human production activities and other endeavours.

By employing a new approach that integrates the Gini coefficient with the number of dry days, we were able to capture not only the uneven distribution of precipitation but also the influence of dry-day frequency on temporal concentration. This method offers a more comprehensive assessment of intra-annual variability. Using this approach, we found that 67.4% of the global land surface exhibited an increasing trend in precipitation concentration over time. This finding aligns closely with conclusions by Dunning et al. (2018) and Liu & Allan (2013), who also observed the widespread presence of the WWDD phenomenon globally^{10,13}. Moreover, the increased concentration of precipitation on a daily scale signifies the need for heightened attention to short-duration intense rainfall events.

Unlike most previous studies that examined temporal or spatial concentration separately, this work uniquely couples both dimensions to reveal a more complete pattern of precipitation distribution. When both the temporal and spatial dimensions increase simultaneously, it indicates a spatiotemporal amplification of the WWDD phenomenon. This could be directly linked to the risk of compound extreme events, such as flooding or drought. Conversely, if the spatial Gini coefficient increases while the temporal Gini coefficient decreases, it may suggest that precipitation is concentrated spatially, but its temporal distribution becomes more uniform. This combined pattern may reflect different climatic mechanisms (e.g., atmospheric circulation changes vs. local evapotranspiration feedback)^{46,47}. Additionally, there could be a coupling relationship, where an increase in temporal concentration (fewer rainy days but higher intensity) could further amplify spatial concentration through soil moisture-precipitation feedback⁴⁸.

Similar to the study by Liu and Allan, which combines seasonal and spatial perspectives, we also confirm the presence of WWDD at both temporal and spatial scales across global tropical land areas¹⁰. We categorize global precipitation concentration changes into four spatiotemporal patterns. For our research, regions such as NEAF and SEAF exhibited a decreasing precipitation trend, indicating that the WWDD_{Spatial-Temporal} phenomenon is achieved primarily via a significant reduction in precipitation on dry days (or in dry areas). This also creates other problems, such as increases in the intensity of heavy precipitation days, which often occurs at the expense of moderate or light precipitation days, either in terms of intensity or frequency^{21,43,44}. In addition to addressing the risks of extreme precipitation, a reduction in light precipitation decreases the removal of aerosols, which further affects cloud formation and the absorption of solar radiation, thereby influencing the climate and posing threats to human health^{45,46}. Conversely, in regions such as SEA, where precipitation increases, the mechanism underlying the WWDD_{Spatial-Temporal} phenomenon is driven by a greater increase in the number of heavy precipitation days. Therefore, these regions face a heightened risk of flooding that requires increased attention. The WDDW_{Spatial-Temporal} pattern is primarily concentrated in high-latitude regions of the Northern Hemisphere, where precipitation is more evenly distributed both throughout the year and across regions, rendering these regions more suitable for human production activities.

Regions where wet days are becoming wetter but wet areas are becoming drier mainly occur in the Southern Hemisphere (WWDD_{Temporal}). In these regions, attention should be given to the occurrence of extreme precipitation and drought events throughout the year. In regions where wet days are becoming drier and wet areas are becoming wetter (WWDD_{Spatial}) the focus should be on the risk of natural disasters such as floods and mudslides triggered by precipitation convergence.

This study provides a new perspective by applying the Gini coefficient to quantify changes in precipitation distribution across both temporal and spatial scales. By identifying WWDD and WDDW patterns at finer resolutions, we reveal pronounced regional differences in precipitation patterns, which give rise to distinct water-related risks. Building on this, we integrate temporal and spatial dimensions to further classify shifts in precipitation patterns, thereby informing the development of more targeted and region-specific adaptation strategies. This integrated framework improves our understanding of evolving precipitation dynamics and offers a robust basis for more effective climate change responses.

Data availability

ERA5-land monthly averaged data is available at <https://cds.climate.copernicus.eu/datasets/derived-era5-land-daily-statistics?tab=overview>.

Code availability

<https://github.com/XinhaoSuo-Theo/WWDD>.

Received: 28 February 2025; Accepted: 3 September 2025

Published online: 26 September 2025

References

- Pendergrass, A. G., Knutti, R., Lehner, F., Deser, C. & Sanderson, B. M. Precipitation variability increases in a warmer climate. *Sci. Rep.* **7**, 17966. <https://doi.org/10.1038/s41598-017-17966-y> (2017).
- Held, I. M. & Soden, B. J. Robust responses of the hydrological cycle to global warming. *J. Clim.* **19**, 5686–5699. <https://doi.org/10.1175/JCLI3990.1> (2006).
- Davenport, F. V., Burke, M. & Diffenbaugh, N. S. Contribution of historical precipitation change to US flood damages. *Proc. Natl. Acad. Sci.* **118**, e2017524118. <https://doi.org/10.1073/pnas.2017524118> (2021).
- Kotz, M., Levermann, A. & Wenz, L. The effect of rainfall changes on economic production. *Nature* **601**, 223–227. <https://doi.org/10.1038/s41586-021-04283-8> (2022).
- Willner, S. N., Otto, C. & Levermann, A. Global economic response to river floods. *Nat. Clim. Change* **8**, 594–598. <https://doi.org/10.1038/s41558-018-0173-2> (2018).
- Damania, R. J. O. R. o. E. P. The economics of water scarcity and variability. *36*, 24–44 (2020).
- Desbureaux, S. & Rodella, A. S. Drought in the city: the economic impact of water scarcity in Latin American metropolitan areas. *World Dev.* **114**, 13–27. <https://doi.org/10.1016/j.worlddev.2018.09.026> (2019).
- He, C. et al. Future global urban water scarcity and potential solutions. *Nat. Commun.* **12**, 4667. <https://doi.org/10.1038/s41467-021-25026-3> (2021).
- Schewe, J. et al. Multimodel assessment of water scarcity under climate change. *Proc. Natl. Acad. Sci.* **111**, 3245–3250. <https://doi.org/10.1073/pnas.1222460110> (2014).
- Liu, C. & Allan, R. P. Observed and simulated precipitation responses in wet and dry regions 1850–2100. *Environ. Res. Lett.* **8**, 034002. <https://doi.org/10.1088/1748-9326/8/3/034002> (2013).
- Zhou, S. et al. Diminishing seasonality of subtropical water availability in a warmer world dominated by soil moisture–atmosphere feedbacks. *Nat. Commun.* **13**, 5756. <https://doi.org/10.1038/s41467-022-33473-9> (2022).
- Chou, C. et al. Increase in the range between wet and dry season precipitation. *Nat. Geosci.* **6**, 263–267. <https://doi.org/10.1038/ngeo1744> (2013).
- Dunning, C. M., Black, E. & Allan, R. P. Later wet seasons with more intense rainfall over Africa under future climate change. *J. Clim.* **31**, 9719–9738. <https://doi.org/10.1175/JCLI-D-18-0102.1> (2018).
- Zhang, Y., Fueglistaler, S. & Mechanism for Increasing Tropical Rainfall Unevenness With Global Warming. *Geophys. Res. Lett.* **46**, 14836–14843. <https://doi.org/10.1029/2019GL086058> (2019).
- Greve, P. et al. Global assessment of trends in wetting and drying over land. *Nat. Geosci.* **7**, 716–721. <https://doi.org/10.1038/ngeo2247> (2014).
- Yang, T., Ding, J., Liu, D., Wang, X. & Wang, T. Combined use of multiple drought indices for global assessment of dry gets drier and wet gets wetter paradigm. *J. Clim.* **32**, 737–748. <https://doi.org/10.1175/JCLI-D-18-0261.1> (2019).
- Trancoso, R. et al. Significantly wetter or drier future conditions for one to two thirds of the world's population. *Nat. Commun.* **15**, 483. <https://doi.org/10.1038/s41467-023-44513-3> (2024).
- Zaitchik, B. F., Rodell, M., Biasutti, M. & Seneviratne, S. I. Wetting and drying trends under climate change. *Nat. Water.* **1**, 502–513. <https://doi.org/10.1038/s44221-023-00073-w> (2023).
- Gomis-Cebolla, J., Rattayova, V., Salazar-Galán, S. & Francés, F. Evaluation of ERA5 and ERA5-Land reanalysis precipitation datasets over Spain (1951–2020). *Atmos. Res.* **284**, 106606. <https://doi.org/10.1016/j.atmosres.2023.106606> (2023).
- Giorgi, F. et al. Higher hydroclimatic intensity with global warming. *J. Clim.* **24**, 5309–5324. <https://doi.org/10.1175/2011JCLI3979.1> (2011).
- Muñoz-Sabater, J. et al. ERA5-Land: a state-of-the-art global reanalysis dataset for land applications. *Earth Syst. Sci. Data* **13**, 4349–4383, doi:<https://doi.org/10.5194/essd-13-4349-2021> (2021).
- Bandhauer, M. et al. Evaluation of daily precipitation analyses in E-OBS (v19.0e) and ERA5 by comparison to regional high-resolution datasets in European regions. *Int. J. Climatol.* **42**, 727–747. <https://doi.org/10.1002/joc.2769> (2022).
- Xu, J., Ma, Z., Yan, S. & Peng, J. Do ERA5 and ERA5-land precipitation estimates outperform satellite-based precipitation products? A comprehensive comparison between state-of-the-art model-based and satellite-based precipitation products over Mainland China. *J. Hydrol.* **605**, 127353. <https://doi.org/10.1016/j.jhydrol.2021.127353> (2022).
- Xu, C., Wang, W., Hu, Y. & Liu, Y. Evaluation of ERA5, ERA5-Land, GLDAS-2.1, and GLEAM potential evapotranspiration data over Mainland China. *J. Hydrology: Reg. Stud.* **51**, 101651. <https://doi.org/10.1016/j.jrehr.2023.101651> (2024).
- Jiang, Q. et al. Evaluation of the ERA5 reanalysis precipitation dataset over Chinese Mainland. *J. Hydrol.* **595**, 125660. <https://doi.org/10.1016/j.jhydrol.2020.125660> (2021).
- Li, Q., Jiang, Y., Wei, L., Liu, F. & Zhu, J. Comparison of ERA5-Land and CMPAS reanalysis data for the regional assessment of precipitation in chongqing, China. *Meteorol. Atmos. Phys.* **137**, 16. <https://doi.org/10.1007/s00703-025-01062-2> (2025).
- Rajah, K. et al. Changes to the Temporal distribution of daily precipitation. *Geophys. Res. Lett.* **41**, 8887–8894. <https://doi.org/10.1029/2014GL062156> (2014).
- Zhang, Q., Gu, X., Singh, V. P., Kong, D. & Chen, X. Spatiotemporal behavior of floods and droughts and their impacts on agriculture in China. *Glob. Planet Change* **131**, 63–72. <https://doi.org/10.1016/j.gloplacha.2015.05.007> (2015).
- Polade, S. D., Pierce, D. W., Cayan, D. R., Gershunov, A. & Dettinger, M. D. The key role of dry days in changing regional climate and precipitation regimes. *Sci. Rep.* **4**, 4364. <https://doi.org/10.1038/srep04364> (2014).
- Iturbide, M. et al. An update of IPCC climate reference regions for Subcontinental analysis of climate model data: definition and aggregated datasets. *Earth Syst. Sci. Data* **12**, 2959–2970. <https://doi.org/10.5194/essd-12-2959-2020> (2020).
- Shepherd, T. G. Atmospheric circulation as a source of uncertainty in climate change projections. *Nat. Geosci.* **7**, 703–708. <https://doi.org/10.1038/ngeo2253> (2014).
- Bhatnagar, S. et al. Exploring the dynamics of climate-smart agricultural practices for sustainable resilience in a changing climate. *Environ. Sustain. Indic.* **24**, 100535. <https://doi.org/10.1016/j.indic.2024.100535> (2024).
- Newman, R. & Noy, I. The global costs of extreme weather that are attributable to climate change. *Nat. Commun.* **14**, 6103. <https://doi.org/10.1038/s41467-023-41888-1> (2023).
- Seppelt, R., Klotz, S., Peiter, E. & Volk, M. Agriculture and food security under a changing climate: an underestimated challenge. *iScience* **25**, 105551. <https://doi.org/10.1016/j.isci.2022.105551> (2022).

35. Audebert, P. et al. Ecological zoning for climate policy and global change studies. *Nat. Sustain.* **7**, 1294–1303. <https://doi.org/10.1038/s41893-024-01416-5> (2024).
36. Deser, C., Phillips, A. S., Alexander, M. A. & Smoliak, B. V. Projecting North American climate over the next 50 years: uncertainty due to internal variability. *J. Clim.* **27**, 2271–2296. <https://doi.org/10.1175/JCLI-D-13-00451.1> (2014).
37. Zhisheng, A. et al. Global monsoon dynamics and climate change. *43*, 29–77, (2015). <https://doi.org/10.1146/annurev-earth-060313-054623>.
38. Wang, W., Pijl, A. & Tarolli, P. Future climate-zone shifts are threatening steep-slope agriculture. *Nat. Food.* **3**, 193–196. <https://doi.org/10.1038/s43016-021-00454-y> (2022).
39. Ajur, S. B. & Al-Ghamdi, S. G. Exploring urban growth–climate change–flood risk nexus in fast growing cities. *Sci. Rep.* **12**, 12265. <https://doi.org/10.1038/s41598-022-16475-x> (2022).
40. Andimuthu, R. et al. Performance of urban storm drainage network under changing climate scenarios: flood mitigation in Indian coastal City. *Sci. Rep.* **9**, 7783. <https://doi.org/10.1038/s41598-019-43859-3> (2019).
41. Tran, V. N. et al. Connectivity in urbanscapes can cause unintended flood impacts from stormwater systems. *Nat. Cities.* **1**, 654–664. <https://doi.org/10.1038/s44284-024-00116-7> (2024).
42. Guan, Y. et al. Increase in ocean-onto-land droughts and their drivers under anthropogenic climate change. *Npj Clim. Atmospheric Sci.* **6**, 195. <https://doi.org/10.1038/s41612-023-00523-y> (2023).
43. Feng, S. & Fu, Q. Expansion of global drylands under a warming climate. *Atmos. Chem. Phys.* **13**, 10081–10094. <https://doi.org/10.5194/acp-13-10081-2013> (2013).
44. Hirabayashi, Y. et al. Global flood risk under climate change. *Nat. Clim. Change.* **3**, 816–821. <https://doi.org/10.1038/nclimate1911> (2013).
45. Jin, K., Wu, Y., Sun, X., Sun, Y. & Gao, C. Spatial–temporal assessment of future extreme precipitation and extreme high-temperature exposure across China. *Int. J. Climatol.* **44**, 2265–2282. <https://doi.org/10.1002/joc.8452> (2024).
46. Chen, Y., Wang, A., Zhi, R. & Feng, G. Contributions of Large-Scale circulation and local Land–Atmosphere interaction to precipitation in Eastern China: investigation on influencing factors of the July 2021 heavy precipitation event in Henan Province. *Chin. J. Atmospheric Sci.* **47**, 551–566. <https://doi.org/10.3878/j.issn.1006-9895.2208.21239> (2023).
47. Yang, Y. et al. Evapotranspiration on a greening Earth. *Nat. Reviews Earth Environ.* **4**, 626–641. <https://doi.org/10.1038/s43017-023-00464-3> (2023).
48. Zan, B., Wang, H., Wei, J. & Song, Y. Temporal and Spatial soil Moisture–Precipitation coupling relationships over the Tibetan plateau. *J. Geophys. Research: Atmos.* **129**, e2023JD040621. <https://doi.org/10.1029/2023JD040621> (2024).

Author contributions

Conceptualization: BL, BFMETHODOLOGY: BF, XSInvestigation: XS, BFVisualization: BF, XS, YJ, GC, JLFunding acquisition: BL, BFSupervision: BL, BFWriting – original draft: XS, BFWriting – review & editing: BF, XS, YJ, GC, YL, JL, LL, ML, XW, BL.

Funding

National Key R&D Program of China grant 2022YFF0802503 and National Natural Science Foundation of China grant 42201515.

Declarations

Competing interests

The authors declare no competing interests.

Additional information

Supplementary Information The online version contains supplementary material available at <https://doi.org/10.1038/s41598-025-18721-4>.

Correspondence and requests for materials should be addressed to B.F. or B.L.

Reprints and permissions information is available at www.nature.com/reprints.

Publisher's note Springer Nature remains neutral with regard to jurisdictional claims in published maps and institutional affiliations.

Open Access This article is licensed under a Creative Commons Attribution-NonCommercial-NoDerivatives 4.0 International License, which permits any non-commercial use, sharing, distribution and reproduction in any medium or format, as long as you give appropriate credit to the original author(s) and the source, provide a link to the Creative Commons licence, and indicate if you modified the licensed material. You do not have permission under this licence to share adapted material derived from this article or parts of it. The images or other third party material in this article are included in the article's Creative Commons licence, unless indicated otherwise in a credit line to the material. If material is not included in the article's Creative Commons licence and your intended use is not permitted by statutory regulation or exceeds the permitted use, you will need to obtain permission directly from the copyright holder. To view a copy of this licence, visit <http://creativecommons.org/licenses/by-nc-nd/4.0/>.

© The Author(s) 2025